Langmuir

ARTICLE

pubs.acs.org/Langmuir

Swelling the Hydrophobic Core of Surfactant-Suspended Single-Walled Carbon Nanotubes: A SANS Study

Carlos A. Silvera-Batista and Kirk J. Ziegler*

Department of Chemical Engineering, University of Florida, Gainesville, Florida 32611, United States

Supporting Information

ABSTRACT: Localized solvent environments form around single-wall carbon nanotubes (SWCNTs) because of the ability of surfactant molecules to solubilize immiscible organic solvents. Although these microenvironments around SWCNTs have already been used for fundamental and applied studies, small-angle neutron scattering (SANS) was used here to assess the size and shape of the solvent domains, their uniformity and distribution on the sidewalls, and the effect of solvent swelling on the aggregation state of the suspension. SANS measurements confirm both the formation of local solvent environments and that no irreversible aggregation of the nanotube suspension occurs after the SDS molecules are swollen in solvent. The results also corroborate prior conclusions based on photoluminescence that the structure formed is dependent of the nature of the solvent−surfactant combination; SWCNTs suspended with SDS and swelled with benzene have a more uniform coating on the sidewall than those swelled with *o*-dichlorobenzene. These differences can be important to understanding the effect of the local environment on the photoluminescence properties and the interaction of SWCNTs with interfaces.

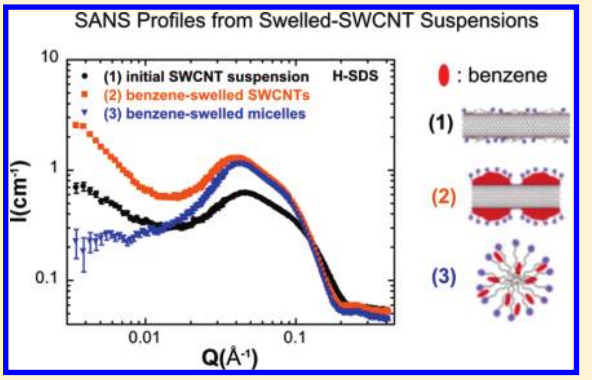

INTRODUCTION

SWCNTs are commonly dispersed in water using synthetic polymers (e.g., Pluronic and Triton X),[1] biopolymers (e.g., DNA,[2] peptides,[3] and gum arabic[4]), and surfactants (e.g., SDS, SDBS, and bile salts).[5−7] After ultracentrifuging these suspensions, the system primarily consists of individual SWCNTs but can also contain small bundles of nanotubes.[5] The surfactant molecules on the surface of a nanotube are mobile and reorganize in response to driving forces, such as high shear stresses[8] and changes in the ionic strength.[9,10] Therefore, the suspending agent and its assembly on the SWCNT surface affects the interfacial properties of SWCNTs. The nature of the interface between the medium and the nanotubes can have significant consequences on the spectroscopic properties of SWCNTs,[11,12] their ability to partition at organic interfaces[13] and agarose,[14] and the density of the surfactant−SWCNT complex.[15]

The ability of surfactants to dissolve hydrophobic molecules can also alter the assembly of surfactants[16] or create localized solvent environments around the SWCNT that can be used to deliver compounds that are insoluble in water to the nanotube surface.[11,16,17] We recently used solvent-induced changes to the surfactant structure to determine the retention mechanism of SDS-suspended SWCNTs on agarose beads.[14] These solvent environments can also be used as microreactors to perform in situ polymerization on the surfaces of SWCNTs[17] or graphene.[18] In a similar approach, Roquelet et al. later used this approach to noncovalently functionalize SWCNTs with porphyrin molecules, demonstrating that porphyrin−SWCNT complexes could be used for the high-yield harvesting of light.[19]

Although these localized environments around SWCNTs have been used for fundamental and applied studies, questions remain about the size and shape of the solvent domains, their uniformity and distribution on the sidewalls, and the effect of solvent swelling on the aggregation state of the suspension. We have chosen to study the structure of the solvent microenvironments around SWCNTs with small-angle neutron scattering (SANS) because it is an excellent technique for probing the structure of soft materials on the nanoscale. At small scattering angles, the small wavelength of neutrons probes length scales from 1 nm to 1 μm.[20,21] Because neutrons interact with other atoms through short-range nuclear interactions, they are a bulk probe that deeply penetrates samples. In addition, the ability to change the contrast factor between the scattering centers and the medium through selective deuteration makes the study of multicomponent or complex samples tractable. In the field of SWCNTs, SANS has been used to measure the dispersion quality of SWCNTs,[22,23] the optimal concentration of dispersing agents,[24] the influence of depletion forces[24] and also enabled studies on the exfoliating power and assembly of polymers on SWCNTs.[25,26] The formation of 3D networks at high SWCNT concentrations[27,28] and in situ polymerization[7,29] processes have also been studied through SANS. Of particular

Received: June 6, 2011
Revised: July 18, 2011

   dx.doi.org/10.1021/la202117p | *Langmuir* XXXX, XXX, 000–000

importance to this study, Yurekli et al. studied the assembly of SDS on SWCNTs and found that the structure of SDS molecules is characterized by a lack of long-range order.[30] In this study, SANS is used to characterize SWCNT suspensions mixed with the immiscible organic solvents benzene and *o*-dichlorobenzene (ODCB). Previously, photoluminescence (PL) data suggested that benzene and ODCB induced the formation of microenvironments with different structural features on the surfaces of nanotubes suspended by SDS.[16] The SANS measurements confirm that nanotubes swelled with ODCB have rough surfaces whereas nanotubes swelled with benzene have smoother surfaces, which are similar to the structures previously inferred using PL spectra.

METHODS

Chemicals. Deionized water (H_2O) and deuterium oxide (D_2O) were used to prepare surfactant solutions as well as SWCNT suspensions. The surfactant, hydrogenated sodium dodecyl sulfate (H-SDS) (99%), and its deuterated counterpart, sodium dodecyl sulfate-d_{25}, D-SDS (98 atom %d), were purchased from Sigma-Aldrich (St. Louis, MO, USA) and used as received. HiPco SWCNTs were obtained from Rice University (Rice HPR 162.3) and used as received. Benzene (99.9%), *o*-dichlorobenzene (99%), and D_2O (99.9 atom % d) were purchased from Sigma-Aldrich. All solvents were used as received. Table 1 shows the scattering length densities (ρ) of all of the chemicals used in the experiments. The values of ρ for the different molecules were calculated from the expression

$$\rho = \frac{\delta N_A}{M}\sum_i b_i \tag{1}$$

where δ is the molecule's bulk density, M is its molecular weight, and b_i is the coherent neutron scattering length of nucleus i.[31]

Aqueous SWCNT Suspensions. Aqueous suspensions of nanotubes were prepared by mixing 40 mg of raw SWCNTs with 100 mL of either 29 mM H- or D-SDS solution. High-shear homogenization (IKA T-25 Ultra-Turrax) for 30 min and ultrasonication (Misonix S3000) for 10 min (120 W) were used to aid all dispersions. During the homogenization and sonication of D_2O-SWCNT suspensions, the beaker and sonicator cup were covered with parafilm to avoid the exchange of D_2O with atmospheric H_2O. After ultrasonication, the mixture was ultracentrifuged at 20 000 rpm (53000*g*) for 4 h using a swing bucket rotor (Beckman Coulter Optima L-80 K, SW-28).

Mixing SWCNT Suspensions with Immiscible Organic Solvents. The swelling of SWCNT suspensions with immiscible organic solvents was performed by following our previously published protocol.[16] Briefly, the suspension was mixed with the organic solvent and vigorously agitated for 30 s in a vortex stirrer. The solvent-swelled suspensions were then left to settle overnight to allow bulk-phase separation prior to scattering experiments. Then, an aliquot of 0.5 mL was carefully withdrawn from the aqueous phase containing swelled SWCNTs to avoid further emulsification. In some cases, the solvent was removed by evaporation at room temperature for 24 h, which was previously shown to remove the solvent encasing the SWCNTs.[16]

SWCNT Characterization. All SWCNT suspensions were characterized by vis−NIR absorbance and NIR−fluorescence spectroscopy using an Applied NanoFluorescence Nanospectralyzer (Houston, TX) with excitation from 662 and 784 nm diode lasers. SANS measurements were performed on the NG3 30 m instrument at the Center for Neutron Research (NCNR) at the National Institute of Standards and Technology (NIST). The wavelength of the neutron beam was 6 Å. Three sample-to-detector distances were used (1, 4, and 13.2 m) to obtain a scattering vector (Q) range from 0.003 to 0.4 Å^{-1}. The samples were loaded into demountable titanium cells with quartz windows that had a path length of 1 mm. Multiple samples (up to 10) were placed on a sample rack for SANS measurements. An empty cell and a blocked beam transmission measurement were used to convert the data to an absolute scale.

Table 1. Scattering-Length Densities of All Chemicals Used in This Study

chemical	ρ (10^{10} cm^{-2})
H_2O	−0.56
D_2O	6.39
H-SDS	0.387
D-SDS	6.704
H-benzene	1.18
H-ODCB	2.35
SWCNT[28]	4.9

Data Analysis. The magnitude of the scattering vector (Q) is a function of the scattering angle (θ) and the neutron wavelength (λ) as given by

$$Q = \left(\frac{4\pi}{\lambda}\right)\sin\left(\frac{\theta}{2}\right) \tag{2}$$

The scattering intensity can be decoupled into intra- and interparticle contributions, and in the case of an incompressible system, it can be modeled as

$$I(Q) = \left(\frac{N}{V}\right)V_p{}^2\Delta\rho^2 P(Q)\,S(Q) + I_{Inc} \tag{3}$$

where N/V, V_p and $\Delta\rho$ are the number density of particles, the particle volume, and contrast factor, respectively. I_{inc} is a constant that describes the incoherent scattering from the sample. The single-particle form factor, $P(Q)$, and the structure factor, $S(Q)$, are dimensionless functions. $P(Q)$ depends on the size and shape of the scattering particles, whereas $S(Q)$ depends on the degree of local order and the interaction potential between the scattering particles.

The micelles in the SDS solution can be modeled as either triaxial or uniform ellipsoids. Prévost and Gradzielski found that a triaxial ellipsoid model was necessary to fit SANS and SAXS data of SDS or CTAB surfactant solutions simultaneously.[32] However, at the low salt concentrations used in this study, SDS solutions can be fit to a uniform ellipsoid.[33] The form factor for a uniform ellipsoid, with semiminor axis a and semimajor axis b, was calculated through the following expression

$$P(Q) = \frac{Y}{V_{ell}}(\rho_{ell} - \rho_{solv})\int_0^1 f^2(Q,x)\,dx \tag{4}$$

$$f(Q,x) = 3V_{ell}\left(\frac{\sin u - u\cos u}{u^3}\right)^2 \text{ and} \tag{5}$$

$$u = Qb[a^2x^2 + b^2(1-x^2)]^{1/2} \tag{6}$$

where the ellipsoid volume is $V_{ell} = (4\pi/3)ab^2$. Because of their size and surface charge, SDS micelles can be considered to be macroions. The structure factor was modeled by assuming that SDS micelles interact only through a repulsive potential. The Coulomb potential that results from the mutual interaction of the micelle's double-layer determines the repulsive potential.[34,35]

Fits to the data were calculated in Igor Pro using the SANS analysis package provided by the NCNR. For pure micelles or those modified with NaCl, the fitting parameters were the volume fraction, the incoherent background, a, b, and the micellar charge. The concentration of monovalent salt was the critical micelle concentration (cmc) for pure SDS solutions. When NaCl was added to solutions of SDS, the total salt concentration was assumed to be the sum of the cmc and the

dx.doi.org/10.1021/la202117p |*Langmuir* XXXX, XXX, 000–000

concentration of NaCl. The dielectric constant of the medium was assumed to be that of water. In the case of micelles swelled with solvents, the scattering-length density of the micelles was allowed to vary. The quality of the fit was evaluated from $\chi_r^2 = [\chi^2/(N - f - 1)]^{1/2}$, with N and f being the number of data points and fitting parameters, respectively. χ^2 is defined as the sum of the squares of the deviation of the data, I_i, from the fitting function, $I(Q)$, normalized by the standard deviation of each data point, $\chi^2 \equiv \Sigma_i((I_i - I)/\sigma_i)^2$.

RESULTS

A suspension of SWCNTs in an aqueous solution of H-SDS is expected to produce scattering from the free surfactant micelles and the SDS/SWCNT complex. Figure 1 shows the scattering from an SDS-coated SWCNT suspension and an SDS solution (i.e., without nanotubes). At high Q (>0.02 Å^{-1}), the signal from the SDS solution is characterized by a structure peak (0.05 Å^{-1}) and a shoulder (0.5 Å^{-1}) typical of ionic surfactant solutions.[32,33] A rising scattering intensity is observed in the low-Q range (<0.02 Å^{-1}). When SWCNTs are dispersed with the aid of SDS, the scattering intensity in the high-Q range does not change substantially. The scattering intensity of the SWCNT suspension in the high-Q range is slightly lower than that from the SDS solution (only SDS micelles and monomers). The lower intensity might be due to the removal of SDS molecules during ultracentrifugation or the adsorption of SDS molecules on SWCNTs. However, there is a remarkable difference between the scattering from the SDS solution and the SWCNT suspension at the low-Q range. These differences can be attributed only to the presence of SWCNTs.

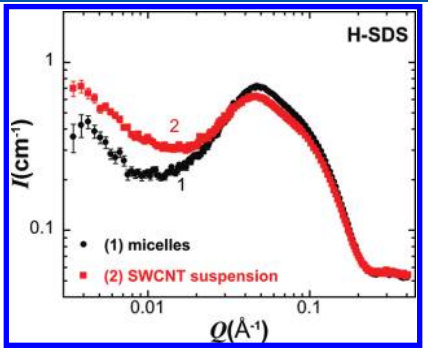

Figure 1. SANS scattering intensity from (1) SDS micelles and (2) SWCNTs suspended in SDS.

H-SDS-suspended SWCNTs were then swelled with H-benzene, and their scattering was measured. Figure 2a shows the scattering from the benzene-swelled SWCNT suspensions and the respective benzene-swelled micelles. The intensity of the SWCNT suspension at low- and high-Q values is largely increased when compared to the initial suspension. The structure peak also shifts to lower Q values. Likewise, the peak position shifts and the scattering intensity in the high-Q regime increases for the SDS micelles mixed with benzene. However, the difference between the scattering profiles from the two samples is large. Surprisingly, the intensity at low Q decreases after the micelles are mixed with benzene. Figure 2b shows the scattering from the ODCB-swelled SWCNT suspensions and the respective ODCB-swelled micelles. Similar to the case of benzene, the intensity of the SWCNT suspension at low- and high-Q values increases when compared to the initial SWCNT suspension. However, changes to the scattering profile are different. Although the intensity at low Q decreases for benzene-swelled micelles, it increases substantially when the SDS solution is mixed with ODCB.

After swelling the micelles or surfactant-coated SWCNTs, the solvents were removed by evaporation. The objective of this experiment was to observe if the contact with organic solvents caused any irreversible effects on the SWCNT suspension. Figure 3 shows that there was an increase in the incoherent background, as indicated by the signal at values of Q higher than 0.2 Å^{-1}. This behavior is expected because D_2O exchanges with atmospheric H_2O during solvent evaporation. Interestingly, at high-Q values, SWCNT suspensions mixed with solvents return

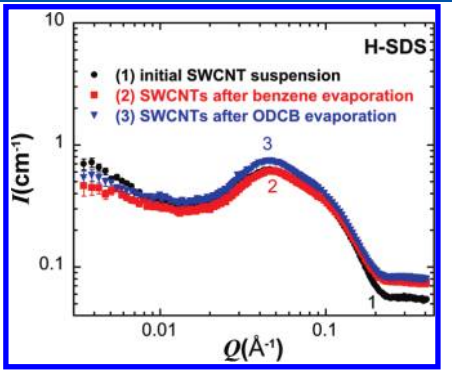

Figure 3. Scattering intensity from the initial SWCNT suspension and after the benzene or ODCB in solvent-swelled SWCNTs has been evaporated.

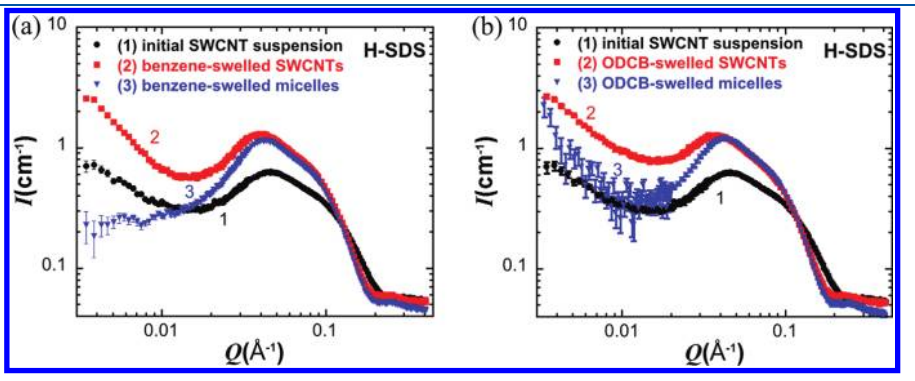

Figure 2. Scattering profile from SWCNT suspensions swelled with (a) benzene and (b) ODCB. The scattering from the initial SWCNT suspension and SDS micelles was plotted for comparison.

dx.doi.org/10.1021/la202117p |*Langmuir* XXXX, XXX, 000–000

Table 2. Parameters Used to Fit the Scattering Data from the SDS Micelles at Varying Salt Concentrations[a]

parameters	H-SDS	0.1 M NaCl	0.2 M NaCl
minor axis (Å)	14.55	14.43	14.62
major axis (Å)	21.55	25.67	28.97
aggregation number, N_{agg}	69.00	97.00	125.00
degree of ionization, z/N_{agg}	0.20	0.17	0.064
χ_r^2	2.21	2.30	1.88

[a] The data was fit to a uniform ellipsoid with the structure factor for a screened Coulomb potential.

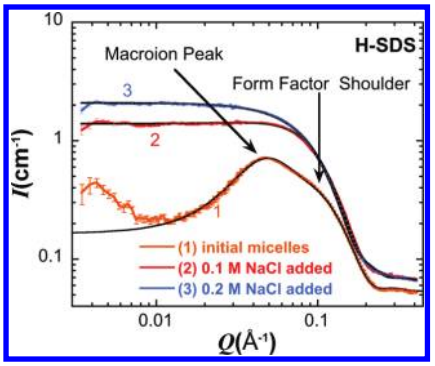

Figure 4. Fit to the scattering data from the SDS micelles at varying salt concentrations. The fit for the initial micelles was performed only for $Q \geq 0.02$ Å^{-1}, and the fit for the other two samples covered the whole Q range.

to their initial state after the evaporation process. In the case of benzene-swelled SWCNTs, the peak position and intensity matches the initial SWCNT suspension in the high-Q range. The peak position also returns to higher Q values for the suspension swelled with ODCB; however, the intensity does not completely match that of the initial suspension. In the low-Q range, the slope of the scattering intensity decreases for both suspensions after evaporation when compared to either the initial suspension or their solvent-swelled counterparts.

DISCUSSION

SDS Micelles. It is well known that SDS molecules self-assemble into aggregates (micelles) once the critical micelle concentration (cmc) is reached.[36] In water, the charges on the SDS molecules dissociate. Therefore, micelles can be considered to be macroions that interact with each other through Coulombic interactions. All of these features are evident in the SANS scattering profile of the SDS solution. At the highest Q values, the major contribution to SANS intensity comes from the form factor, which is a function of the size and shape of the SDS micelles. The peak at 0.05 Å^{-1}, which corresponds to 130 Å in real space, is due to the Coulombic interaction among micelles. These features can be modeled using an oblate or uniform ellipsoid form factor and the screened Coulomb potential for macroions.

Table 2 shows the geometrical and physical parameters obtained from a fit to the 1 wt % SDS micellar solution; the resulting curve is shown in Figure 4. The micelles show minor and major axes of 14.5 and 21.5 Å, respectively, which are in agreement with previously published data.[32,33] From the volume

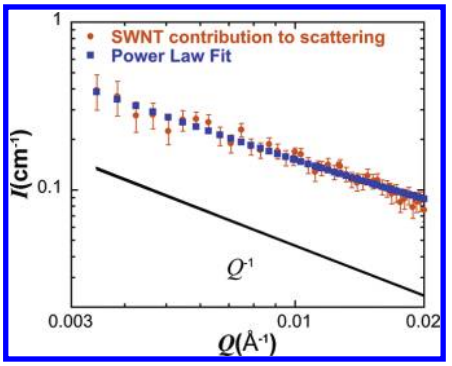

Figure 5. SWCNT contribution to scattering after subtracting the contribution from the SDS micelles. The scattering intensity of SDS micelles was multiplied by a factor of 0.86 to match the intensities of the peaks at Q = 0.05 Å^{-1} prior to subtraction. The resulting data is described by a function of the form $I(Q) = (1.5 \times 10^{-3})Q^{-0.97} + 2.2 \times 10^{-2}$ with $\chi_r^2 = 0.97$. A $Q^{-1.2}$ dependence is obtained if the raw scattering intensity of SDS micelles is used instead.

of the micelles, an aggregation number of 69 SDS molecules/micelle can be calculated using the molecular volume of SDS, 0.41 nm^3, as reported by Prévost and Gradzielski.[32] Likewise, this result is in agreement with values of the micellar aggregation numbers previously reported for SDS in aqueous solutions.[33,37]

It is possible that the rising signal at low Q is due to the clustering or nonuniform distribution of SDS micelles, as previously suggested by Wang et al.[24] and extensively described in the case of polymer solutions.[38,39] An experiment performed with a solution of D-SDS instead of H-SDS shows that the intensity at high Q becomes flat, as expected because the micelles are contrast-matched (Figure S1 in Supporting Information). However, the rising intensity at low Q still appears. This behavior suggests the low-Q intensity has its origins in density fluctuations of the system, which are a manifestation of clustering.[21,39] To probe the nature of the signal in this region further, the ionic strength of the H-SDS micelle solution was changed by adding NaCl. As the concentration of NaCl increases, Figure 4 shows that the polyelectrolyte peak disappears because the charges on SDS micelles are screened. Likewise, the elimination of the rising signal at low Q indicates that Coulombic interactions play a significant role in creating a nonuniform distribution of scattering centers in the solution. The results in Table 2 also show that the micelles grow in size and asymmetry when screened by NaCl.

SWCNT Suspension. SANS is very sensitive to the aggregation state of SWCNTs.[22,24,40] Therefore, the interpretation of the results on solvent-swelled SWCNTs depends on the initial state of the suspension. Although some have questioned the ability of SDS to exfoliate and individually suspend SWCNTs,[41−43] especially large-diameter nanotubes, Quinton and co-workers[44] showed that SDS is effective in dispersing nanotubes with an average diameter of 1 nm, such as those produced through the HiPco process. The scattering intensity from rigid rods is characterized by $I \propto Q^{-1}$ behavior whereas aggregated rods appear as mass fractals that exhibit a $Q^{-2.5}$ dependence.

Figure 5 shows the contribution of SWCNTs to the scattering intensity after subtracting the intensity from the SDS micelles. Only the data up to 0.02 Å^{-1} is shown because the signal is completely dominated by the SDS micelles above this Q range. The data can be described by a power law function with an exponent of −0.97, which is the relationship expected of

dx.doi.org/10.1021/la202117p |Langmuir XXXX, XXX, 000–000

well-dispersed rigid rods. This data strongly suggests that SWCNTs in this particular system (HiPco SWCNTs) behave as rigid rods, which is in agreement with the results of Quinton and co-workers.[44] In other words, the suspension seems to be composed primarily of individual SWCNTs and a marginal number of small bundles. The absence of a strong signal from the SWCNTs or the surfactant−SWCNT complexes at high-Q values indicates that surfactant molecules do not form well-organized aggregates on the nanotube sidewall. This is in agreement with Yurekli et al.,[30] who performed a detailed SANS study on the assembly of SDS on SWCNTs and found that the scattering intensity at high Q could not be fit to any combination of the scattering from interacting spheres (micelles) and SWCNTs coated with cylindrical micelles.

Effects of Solvent Solubilization on SDS Micelles. Although the solubility of the two organic solvents in pure water is small (1.77 g/L for benzene and 0.15 g/L for ODCB),[45] their solubility increases linearly with the concentration of SDS micelles.[46,47] The hydrophobic micelle core, the surfactant palisade (area between the polar head and the hydrophobic core), and even the polar head serve as loci of solubilization for aromatic compounds, as shown in Figure 6.[48,49] The partitioning of the two solvents between water and micelles is characterized by the micelle−water phase distribution coefficient, K_{XM}, which is defined as the ratio of mole fractions in the micellar and aqueous phases.[46,50] The log K_{XM} values for benzene and ODCB in SDS solutions are approximately 3 and 3.89.[50] Using the concentration of SDS from our experiments and the given values of log K_{XM}, the solubility of benzene and ODCB increases by factors of 1.4 and 4.7, respectively. These large increases in solubility should affect the volume, symmetry, and aggregation number of the micelles.[47] These changes are expected because of the hydrophobic volume changes during solubilization, as explained further below. Note that the solubilization of an organic compound is a different phenomenon from the spontaneous formation of microemulsions. In the latter case, the solvent forms a segregated region in the hydrophobic core of the micelle. In the former, the micelles are swelled because the solute can be located at different points within the micelle depending on their structure. It was previously mentioned that the intensity from SDS micelles increases in the high-Q regime as the solution is mixed with ODCB and benzene. It is likely that the large changes in intensity correspond to changes in the size of the SDS micelles and consequently the number of charges. Table 3 shows the geometrical parameters of the SDS micelles in the presence of solvents. It is observed that the major and minor axes of the micelle increase, which results in volume changes of 62 and 72% for benzene and ODCB, respectively.

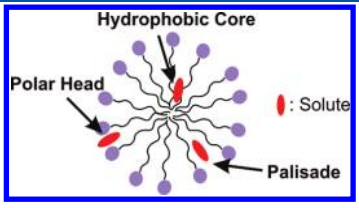

Figure 6. Loci of solubilization for organic compounds in SDS micelles.

Table 3. Parameters Used to Fit the Scattering from Swelled SDS Micelles[a]

parameters	benzene	ODCB
minor axis (Å)	17.75	18.19
major axis (Å)	25.67	26.5
charge, z	19.14	19.32
χ_r^2	2.41	1.95

[a] The data was fit to a uniform ellipsoid with the structure factor for a screened Coulomb potential. The concentration of free ions was 0.008 M, which is close to the critical micelle concentration.

Effects of Solvent Solubilization on SWCNT Suspensions. Once again, the scattering intensity from swelled micelles must be subtracted from the scattering behavior of nanotubes after solvent swelling to obtain the scattering from only the swelled SWCNTs. Figure 7 shows the resulting scattering profile for SWCNT suspensions mixed with benzene and ODCB. An important question is whether the aggregation state of the SWCNT suspension changes as it is swelled with the organic solvents. The low-Q signal has a $Q^{-2.5}$ and Q^{-1} form for benzene and ODCB, respectively. This change in slope suggests that SWCNTs in the suspension aggregate after swelling with benzene. However, there is no visible sign of aggregation in the suspensions, and PL and absorbance spectra do not show signs of aggregation either (not shown). A further complication to the analysis of these changes is that ODCB-swelled SWCNTs have Q^{-1} and $Q^{-2.5}$ dependencies when suspended in H-SDS and D-SDS solutions, respectively. Significant differences in this low-Q region were also observed in swelled-micelles (i.e., no SWCNTs) as shown in Figure 2. Although it is difficult to determine the aggregation state of the swelled SWCNT suspensions, it is important to note that the scattering at low Q returns to a similar intensity once benzene and ODCB are evaporated, as shown in Figure 3. Once the solvent is evaporated and the contribution from SDS

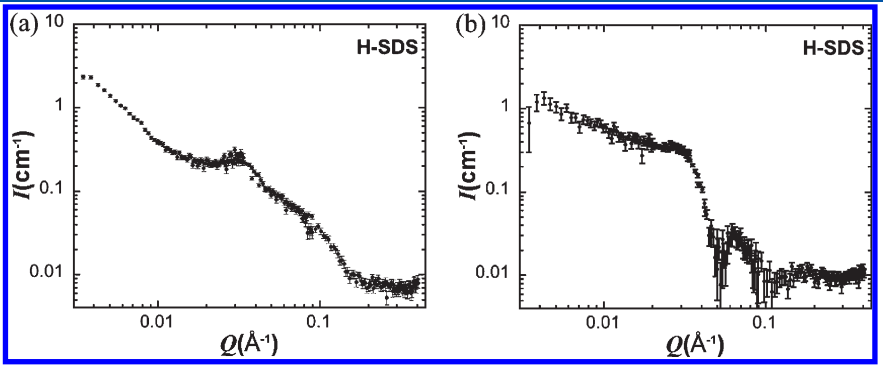

Figure 7. Scattering from (a) benzene- and (b) ODCB-swelled SWCNT suspensions after the scattering from the swelled SDS micelles was subtracted.

dx.doi.org/10.1021/la202117p |Langmuir XXXX, XXX, 000–000

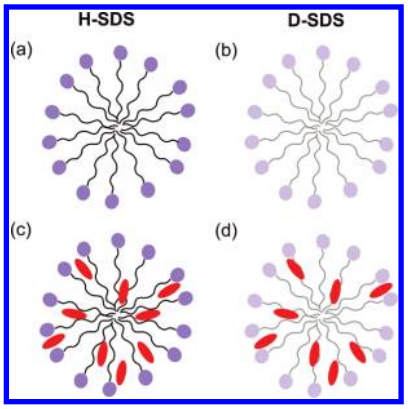

Figure 8. Schematic representation of the (a, b) initial and (c, d) swelled surfactant micelles for (a, c) hydrogenated and (b, d) deuterated SDS.

micelles is subtracted, the slope at low Q returns to values of close to −1 for both compounds. This reversibility was also observed in prior spectroscopy experiments[16] and suggests that the swelling process and any changes to the aggregation state are reversible.

Figure 7 also shows a new feature for SWCNT suspensions mixed with both benzene and ODCB in the high-Q range. This result is in stark contrast to the results from SDS-coated SWCNTs, which show no structure on the SWCNT sidewall. Because the signal from the swelled micelles was subtracted, it is probable that the structure producing the excess scattering is on the SWCNT sidewall. According to the Q range that is being probed, the structure has a characteristic length scale of at least 15 Å. It is highly probable that these microstructures consist of both an organic solvent and SDS molecules because the removal of SDS molecules would lead to the aggregation of SWCNTs because of the loss of the repulsive electrostatic interactions.

The features of these microstructures are potentially dependent on the nature of the solvent. When describing the structure and self-assembly behavior of surfactants into micelles, the nondimensional packing parameter, $v/a_o l_a$, is frequently used, where v is the hydrocarbon (hydrophobic) volume, a_o is the interfacial (polar) area, and l_a is the critical or alkyl chain length.[36] The value of the packing parameter determines the micelle characteristics, including whether a surfactant assembles into spherical or cylindrical micelles. The value of the packing parameter can be modified by adjusting any of these parameters, such as changing the value of a_o by using salt to screen the charges on the surfactant molecules. The changes observed in Figure 4 and Table 3 are a direct consequence of the changes in the packing parameter upon salt addition. More relevant to our experiments is the fact that v can also be changed by the solubilization of aromatic compounds into SDS micelles. The presence of the aromatic compounds can change the contribution of the hydrophobic volume to the packing parameter. However, these effects are dependent on the aromatic species and the dominant locus of solubilization. For example, it was found that the response of cetylpyridinium bromide (CPB), which forms cylindrical micelles, to the solubilization of hydrocarbons was dependent on the locus of solubilization.[51] The compounds that were preferably localized in the polar head region caused an increase in the aggregation number whereas those that were solubilized in the hydrophobic core simply swelled the CPB micelles. In a similar approach, the packing parameter can also be used as a guide to understand the assembly of surfactants on solid surfaces, such as SWCNT sidewalls.[52] Because benzene and ODCB have different molar volumes and loci of solubilization in SDS micelles, these two solvents could potentially induce the formation of microstructures with different characteristics on the surfaces of SWCNTs.

Characterizing Solvent Microstructures on the SWCNT Sidewall. The results in Figure 7 suggest that small domains of solvent are associated with the SWCNTs. Therefore, D-SDS was used in similar experiments to eliminate the scattering from the SDS micelles. Once all of the H atoms are replaced by D atoms in the SDS molecule, the scattering above 0.02 $Å^{-1}$ becomes flat, indicating that the main contribution to the intensity in this region comes from the incoherent background (data not shown). However, the signal at low Q matches for both samples. These results confirm that micelles are contrast matched when SDS is deuterated, as shown in Figure 8.

Figure 9 shows the scattering profile from a D-SDS solution mixed with benzene and ODCB. The signal at high Q is mostly background, although a very weak peak is observed at around 0.04 $Å^{-1}$ for benzene. This indicates that neither ODCB nor benzene forms an aggregate structure with characteristic lengths of at least 15 Å inside the micelles. Instead, these solvents are distributed throughout the micelle. Likewise, the flat profile in the high-Q region in the initial SWCNT suspension indicates there are no aggregate structures on the SWCNT sidewall. However, aggregate structures become visible once the solvents are added. When SWCNTs coated with D-SDS are swelled with benzene, a distinct peak is observed that confirms that the solvent is forming a microstructure around the SWCNTs. In the case of ODCB, the peak is not as distinct as in the benzene-swelled suspensions but is still visible. Notice that the peak is observed only when nanotubes are present. Although the solvents do not induce considerable structural changes in SDS micelles, they do cause a visible effect on the SWCNT sidewall. The data in Figure 9 strongly suggests that the solvents form aggregates on the SWCNT surface, as shown in Figure 10. As discussed above, the solvents act as a reorganizing force for the surfactants on the SWCNTs.

A correlation length model has been used to fit the data at low and high Q. The model has the following form,

$$I = \frac{A}{Q^m} + \frac{C}{1 + (Q\xi)^n} + I_{inc} \qquad (7)$$

where A and C are two real coefficients, ξ is the correlation length, and m and n are the Porod and Lorentzian exponents for the low- and high-Q regions, respectively.[39] The two terms in eq 7 are additive because they account for structural features on different length scales. In other words, if one were to look at the system at different magnifications, the structural features manifested at low and high Q could not be observed at the same time. The m exponent is related to the mass fractal dimension of the system at low Q. In the case of polymers, the correlation length is the distance between the two points at which a polymer chain is intersected by two other chains. The previous interpretation cannot be translated directly into our system nor can an unambiguous interpretation be found independently of the values of n and m. The regime of interest in our systems is the high-Q region. In our system, exponent n is related to the fractal dimension (D_s) of a surface. In a surface fractal, the surface area S_f within a sphere of radius R follows $S_f(R) \propto R^{D_s}$, where D_s is

dx.doi.org/10.1021/la202117p |*Langmuir* XXXX, XXX, 000–000

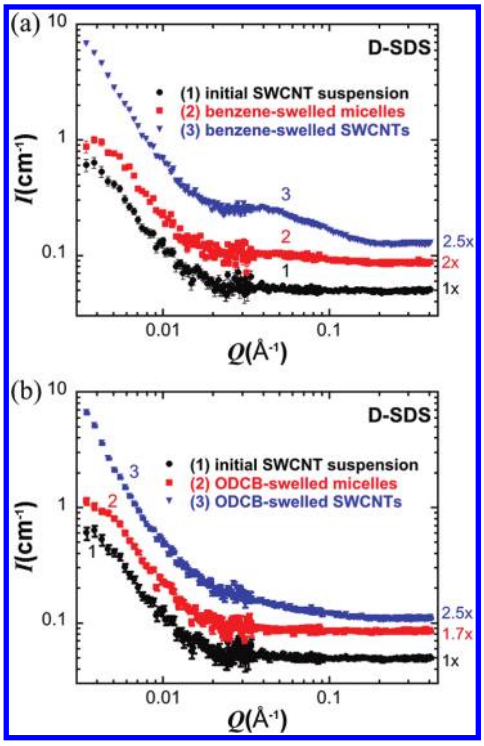

Figure 9. Effect of (a) benzene and (b) ODCB solvent swelling on the scattering intensity from SWCNTs suspended in D-SDS. Scattering from swelled micelles is included for comparison. The curves are offset for clarity. The scattering from swelled SWCNTs after subtraction of the contribution from swelled micelles, as well as the fits to eq 7, are shown in Figures S2 and S3.

related to n by $D_s = 6 - n$. The value of D_s varies between 2 and 3. A smooth surface has $D_s = 2$ ($n = 4$), and the roughness of the surface increases as D_s becomes larger (or n becomes smaller).[21,53]

Table 4 shows the fitting parameters for the scattering data in Figure 9 for SWCNTs suspended in D-SDS after swelling with either benzene or ODCB. The correlation length (ξ) and n have the most significant differences between the two swelled systems. The correlation length in our case can be interpreted as the average distance between solvent aggregates on the SWCNT surface. The correlation length for benzene is 12.02 Å, which is 40% lower than the value for the ODCB system. Figure 10b illustrates the possible structures that are measured in SANS scattering. Specifically, the correlation length could correspond to the distance between domains oriented radially (L_1), axially (L_2), or between SWCNTs (L_3). Although L_1 and L_3 cannot be conclusively disregarded, it is possible to argue that L_2 is the correlation length being measured in the scattering data. If $\xi = L_1$, then the correlation length measured for benzene is too small because the average diameter of the nanotubes in this sample should be approximately 10 Å. The correlation length L_1 would suggest that no benzene is surrounding the nanotube, which is contrary to the scattering results presented in Figure 9. Because these suspensions are dilute according to the criteria of Doi and Edwards ($cL^3 \approx 0.8$, where c is the number density and L is the average length of the SWCNTs, which is assumed to be 3000 Å),[54] it is highly probable that the average distance between solvent domains on different SWCNTs (L_3) is much larger than the correlation length obtained from the fits. In fact, if SWCNTs are organized in a lattice array, an estimated average distance

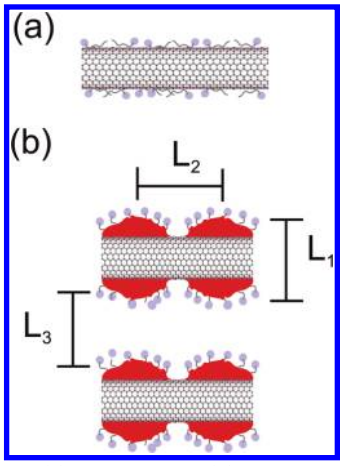

Figure 10. Possible (a) surfactant and (b) solvent structures that form around SWCNTs. The correlation length could potentially be derived from solvent domains on different SWCNTs. L_1, L_2, and L_3 correspond to potential correlation lengths (ξ) measured in SANS scattering. The structures are drawn with deuterated surfactants.

Table 4. Parameters Used to Fit the Scattering Data from SWCNTs Coated with D-SDS and Swelled with Benzene and ODCB

parameters	benzene	ODCB
A	4.84×10^{-7}	1.02×10^{-7}
m	2.63	2.82
C	0.04	0.02
ξ	12.02	19.92
n	3.62	3.03
χ_r^2	1.26	0.98

between nanotubes is on the order of 3200 Å. On the basis of the values of the n exponent, the SWCNT suspension swelled with ODCB shows a very rough surface ($n = 3.03$) whereas the surface for nanotubes swelled with benzene is much smoother ($n = 3.62$). In other words, the domains of benzene on SWCNTs are closer to one another than are those for ODCB. This interpretation is in agreement with our previous conclusions based on PL data[16] in which we argued that ODCB increases the permeability of the surfactant layer surrounding the SWCNT, enabling more interaction of the nanotube with protons in the aqueous phase. However, benzene promoted a surfactant—solvent structure that isolated the nanotubes better from the aqueous environment.

CONCLUSIONS

The structure of nonpolar solvent microenvironments and its effect on the aggregation state of SWCNTs suspended by SDS were studied using SANS. It was shown that SWCNTs produced through the HiPco process are well dispersed by SDS and do not form irreversible aggregates after swelling the surfactant shell with organic solvents. These results strongly support our previous conclusion that dramatic changes to the PL spectra of SWCNTs during swelling are due to surfactant reorganization on the nanotube surface. The SANS measurements also demonstrate that the structure formed by the nonpolar solvents and the SDS molecules depends on the nature of the solvent. Combined with

dx.doi.org/10.1021/la202117p |*Langmuir* XXXX, XXX, 000–000

prior PL measurements, these results show that some solvents, such as benzene, form more uniform coatings on the SWCNT sidewall that result in better coverage and higher PL emission. On the contrary, other solvents (e.g., ODCB) induce structures that expose the sidewalls of SWCNTs to the aqueous media, making them susceptible to extrinsic quenching effects that lower PL emission.

■ ASSOCIATED CONTENT

Supporting Information. Scattering intensity of D-SDS solution and scattering from benzene- and ODCB-swelled SWCNT suspensions after subtracting contributions from swelled D-SDS micelles. This material is available free of charge via the Internet at http://pubs.acs.org.

■ AUTHOR INFORMATION

Corresponding Author
*E-mail: kziegler@che.ufl.edu.

■ ACKNOWLEDGMENT

We acknowledge the National Science Foundation (CBET-0853347) for the support of this research. C.A.S.-B. thanks SEAGEP at the University of Florida for their support. We are grateful to Prof. Yiider Tseng for access to the ultracentrifuge and the Richard Smalley Institute at Rice University for supplying SWCNTs. We acknowledge the support of the National Institute of Standards and Technology (NIST), U.S. Department of Commerce, in providing the neutron research facilities used in this work. This work utilized facilities supported in part by the National Science Foundation under agreement no. DMR-0944772. In particular, we thank Dr. Boulem Hammouda at the NIST Center for Neutron Research for his assistance with data collection and fruitful discussions.

■ REFERENCES

(1) Moore, V. C.; Strano, M. S.; Haroz, E. H.; Hauge, R. H.; Smalley, R. E.; Schmidt, J.; Talmon, Y. *Nano Lett.* **2003**, *3*, 1379–1382.
(2) Zheng, M.; Jagota, A.; Semke, E.; Diner, B.; Mclean, R.; Lustig, S.; Richardson, R.; Tassi, N. *Nat. Mater.* **2003**, *2*, 338–342.
(3) Bakota, E. L.; Aulisa, L.; Tsyboulski, D. A.; Weisman, R. B.; Hartgerink, J. D. *Biomacromolecules* **2009**, *10*, 2201–2206.
(4) Bandyopadhyaya, R.; Nativ-Roth, E.; Regev, O.; Yerushalmi-Rozen, R. *Nano Lett.* **2002**, *2*, 25–28.
(5) Islam, M. F.; Rojas, E.; Bergey, D. M.; Johnson, A. T.; Yodh, A. G. *Nano Lett.* **2003**, *3*, 269–273.
(6) O'Connell, M. J.; Bachilo, S. M.; Huffman, C. B.; Moore, V. C.; Strano, M. S.; Haroz, E. H.; Rialon, K. L.; Boul, P. J.; Noon, W. H.; Kittrell, C.; Ma, J.; Hauge, R. H.; Weisman, R. B.; Smalley, R. E. *Science* **2002**, *297*, 593–596.
(7) Wenseleers, W.; Vlasov, I. I.; Goovaerts, E.; Obraztsova, E.; Lobach, A. S.; Bouwen, A. *Adv. Funct. Mater.* **2004**, *14*, 1105–1112.
(8) Silvera-Batista, C. A.; Weinberg, P.; Butler, J. E.; Ziegler, K. J. *J. Am. Chem. Soc.* **2009**, *131*, 12721–12728.
(9) Niyogi, S.; Densmore, C. G.; Doorn, S. K. *J. Am. Chem. Soc.* **2009**, *131*, 1144–1153.
(10) Duque, J. G.; Densmore, C. G.; Doorn, S. K. *J. Am. Chem. Soc.* **2010**, *132*, 16165–16175.
(11) Silvera-Batista, C. A.; Wang, R. K.; Weinberg, P.; Ziegler, K. J. *Phys. Chem. Chem. Phys.* **2010**, *12*, 6990–6998.
(12) Siitonen, A. J.; Tsyboulski, D. A.; Bachilo, S. M.; Weisman, R. B. *Nano Lett.* **2010**, *10*, 1595–1599.
(13) Wang, R. K.; Reeves, R. D.; Ziegler, K. J. *J. Am. Chem. Soc.* **2007**, *129*, 15124–15125.
(14) Silvera-Batista, C. A.; Scott, D. C.; McLeod, S. M.; Ziegler, K. J. *J. Phys. Chem. C* **2011**, *115*, 9361–9369.
(15) Arnold, M. S.; Green, A. A.; Hulvat, J. F.; Stupp, S. I.; Hersam, M. C. *Nat. Nanotechnol.* **2006**, *1*, 60–65.
(16) Wang, R. K.; Chen, W.-C.; Campos, D. K.; Ziegler, K. J. *J. Am. Chem. Soc.* **2008**, *130*, 16330–16337.
(17) Chen, W.-C.; Wang, R. K.; Ziegler, K. J. *ACS Appl. Mater. Interfaces* **2009**, *1*, 1821–1826.
(18) Das, S.; Wajid, A. S.; Shelburne, J. L.; Liao, Y.-C.; Green, M. J. *ACS Appl. Mater. Interfaces* **2011**, *3*, 1844–1851.
(19) Roquelet, R. C.; Lauret, L. J.; Alain-Rizzo, A.-R. V.; Voisin, V. C.; Fleurier, F. R.; Delarue, D. M.; Garrot, G. D.; Loiseau, L. A.; Roussignol, R. P.; Delaire, D. J.; Deleporte, D. E. *ChemPhysChem* **2010**, *11*, 1667–1672.
(20) Roe, R.-J. *Methods of X-ray and Neutron Scattering in Polymer Science*; Oxford University Press: New York, 2000.
(21) Higgins, J. S.; Benoit, H. C. *Polymers and Neutron Scattering*; Oxford University Press: New York, 1996.
(22) Fagan, J.; Landi, B.; Mandelbaum, I.; Simpson, J. *J. Phys. Chem. B* **2006**, *110*, 23801.
(23) Fagan, J. A.; Becker, M. L.; Chun, J.; Nie, P.; Bauer, B. J.; Simpson, J. R.; Hight-Walker, A.; Hobbie, E. K. *Langmuir* **2008**, *24*, 13880–133889.
(24) Wang, H.; Zhou, W.; Ho, D.; Winey, K.; Fischer, J.; Glinka, C.; Hobbie, E. *Nano Lett.* **2004**, *4*, 1789–1793.
(25) Dror, Y.; Pyckhout-Hintzen, W.; Cohen, Y. *Macromolecules* **2005**, *38*, 7828–7836.
(26) Granite, M.; Radulescu, A.; Pyckhout-Hintzen, W.; Cohen, Y. *Langmuir* **2011**, *27*, 751–759.
(27) Hough, L. A.; Islam, M. F.; Hammouda, B.; Yodh, A. G.; Heiney, P. A. *Nano Lett.* **2006**, *6*, 313–317.
(28) Zhou, W.; Islam, M.; Wang, H.; Ho, D.; Yodh, A.; Winey, K.; Fischer, J. *Chem. Phys. Lett.* **2004**, *384*, 185–189.
(29) Kim, T.-H.; Doe, C.; Kline, S.; Choi, S.-M. *Adv. Mater.* **2007**, *19*, 929–933.
(30) Yurekli, K.; Mitchell, C. A.; Krishnamoorti, R. *J. Am. Chem. Soc.* **2004**, *126*, 9902–9903.
(31) Pethrick, R., Dawkins, J. V., Eds. *Modern Techniques for Polymer Characterisation*; J. Wiley: New York, 1999.
(32) Prevost, S.; Gradzielski, M. *J. Colloid Interface Sci.* **2009**, *337*, 472–484.
(33) Bergstrom, M.; Pedersen, J. *Phys. Chem. Chem. Phys.* **1999**, *1*, 4437–4446.
(34) Hayter, J. B.; Penfold, J. *Mol. Phys.* **1981**, *42*, 109–118.
(35) Hayter, J. B.; Penfold, J. *J. Chem. Soc, Faraday Trans. 1* **1981**, *77*, 1851–1863.
(36) Israelachvili, J. *Intermolecular and Surface Forces*, 2nd ed.; Academic Press: Amsterdam, 1991.
(37) Lianos, P.; Zana, R. *J. Colloid Interface Sci.* **1981**, *84*, 100–107.
(38) Hammouda, B. *J. Chem. Phys.* **2010**, *133*, 084901.
(39) Hammouda, B.; Ho, D. L.; Kline, S. *Macromolecules* **2004**, *37*, 6932–6937.
(40) Bauer, B. J.; Becker, M. L.; Bajpai, V.; Fagan, J. A.; Hobbie, E. K.; Migler, K.; Guttman, C. M.; Blair, W. R. *J. Phys. Chem. C* **2007**, *111*, 17914–17918.
(41) Okazaki, T.; Saito, T.; Matsuura, K.; Ohshima, S.; Yumura, M.; Iijima, S. *Nano Lett.* **2005**, *5*, 2618–2623.
(42) Haggenmueller, R.; Rahatekar, S. S.; Fagan, J. A.; Chun, J.; Becker, M. L.; Naik, R. R.; Krauss, T.; Carlson, L.; Kadla, J. F.; Trulove, P. C.; Fox, D. F.; DeLong, H. C.; Fang, Z.; Kelley, S. O.; Gilman, J. W. *Langmuir* **2008**, *24*, 5070–5078.
(43) Moshammer, K.; Hennrich, F.; Kappes, M. M. *Nano Res.* **2009**, *2*, 599–606.
(44) Blanch, A. J.; Lenehan, C. E.; Quinton, J. S. *J. Phys. Chem. B* **2010**, *114*, 9805–9811.

(45) Lide, D. R., Ed. *CRC Handbook of Chemistry and Physics*; CRC Press: Boca Raton, FL, 1999.
(46) Liu, G. G.; Roy, D.; Rosen, M. J. *Langmuir* **2000**, *16*, 3595–3605.
(47) Rosen, M. J. *Surfactants and Interfacial Phenomena*; Wiley-Interscience: New York, 2004.
(48) Mukerjee, P.; Cardinal, J. R. *J. Phys. Chem.* **1978**, *82*, 1620–1627.
(49) Wasylishen, R. E.; Kwak, J. C. T.; Gao, Z.; Verpoorte, E.; MacDonald, B.; Dickson, R. M. *Can. J. Chem.* **1991**, *69*, 822–833.
(50) Sprunger, L.; William E Acree, J.; Abraham, M. H. *J. Chem. Inf. Model.* **2007**, *47*, 1808–1817.
(51) Kumar, S.; Bansal, D.; Kabir-ud-Din *Langmuir* **1999**, *15*, 4960–4965.
(52) Patrick, H. N.; Warr, G. G.; Manne, S.; Aksay, I. A. *Langmuir* **1997**, *13*, 4349–4356.
(53) Somasundaran, P., Ed. *Encyclopedia of Surface and Colloid Science*, 2nd ed.; CRC Press: Boca Raton, FL, 2006; Vol. 5.
(54) Doi, M.; Edwards, S. F. *The Theory of Polymer Dynamics*; Oxford University Press: Oxford, U.K., 1986.